TÜBİTAK

Turkish Journal of Chemistry

http://journals.tubitak.gov.tr/chem/

Research Article

Turk J Chem
(2016) 40: 706 – 719

doi:10.3906/kim-1512-36

Experimental and theoretical investigation of the reaction between CO_2 and carbon dioxide binding organic liquids

Hilal TANKAL[1,2], Özge YÜKSEL ORHAN[3], Erdoğan ALPER[3,*], Telhat ÖZDOĞAN[1], Hakan KAYI[2]

[1]Department of Physics, Amasya University, Amasya, Turkey

[2]Computational Chemistry Laboratory, Chemical Engineering and Applied Chemistry Department, Atılım University, Ankara, Turkey

[3]Department of Chemical Engineering, Hacettepe University, Ankara, Turkey

Received: 08.12.2015 • **Accepted/Published Online:** 07.04.2016 • **Final Version:** 02.11.2016

Abstract: The reaction kinetics of CO_2 absorption into new carbon dioxide binding organic liquids (CO_2BOLs) was comprehensively studied to evaluate their potential for CO_2 removal. A stopped-flow apparatus with conductivity detection was used to determine the CO_2 absorption kinetics of novel CO_2BOLs composed of DBN (1,5-diazabicyclo[4.3.0]non-5-ene)/1-propanol and TBD (1,5,7-triazabicyclo[4.4.0]dec-5-ene)/1-butanol. A modified termolecular reaction mechanism for the reaction of CO_2 with CO_2BOLs was used to calculate the observed pseudo-first–order rate constant k_0 (s^{-1}) and second-order reaction rate constant k_2 (m^3/kmol.s). Experiments were performed by varying organic base (DBN or TBD) weight percentage in alcohol medium for a temperature range of 288–308 K. It was found that k_0 increased with increasing amine concentration and temperature. By comparing using two different CO_2BOL systems, it was observed that the TBD/1-butanol system has faster reaction kinetics than the DBN/1-propanol system. Finally, experimental and theoretical activation energies of these CO_2BOL systems were obtained and compared. Quantum chemical calculations using spin restricted B3LYP and MP2 methods were utilized to reveal the structural and energetic details of the single-step termolecular reaction mechanism.

Key words: Carbon dioxide absorption, carbon dioxide binding organic liquids, fast reaction kinetics, stopped-flow technique, DFT, B3LYP, MP2

1. Introduction

Since carbon dioxide (CO_2) is considered the major greenhouse gas contributing to global warming due to its abundance, efficient and cost-effective CO_2 capture strategies are required to achieve a significant reduction in atmospheric CO_2 levels. The combustion of fossil fuels is the primary source of the increase in atmospheric CO_2 concentrations. Currently, there are three main capture technologies, i.e. postcombustion capture, precombustion capture, and oxy-fuel combustion. The principle of postcombustion capture is separation of CO_2 from the flue gas after the combustion of fossil fuel in order to significantly reduce power plants' CO_2 emissions. The postcombustion capture method is compatible with the existing conventional coal-fired, oil-fired, or gas-fired power plants without requiring substantial changes in basic combustion technology.[1] Flexibility is the main advantage of the postcombustion method. There are several gas separation technologies being investigated for postcombustion capture; they include absorption, adsorption, cryogenic distillation, and membrane separation.[2]

*Correspondence: ealper@hacettepe.edu.tr

One of the most promising technologies for CO_2 capture is the chemical absorption of CO_2 into aqueous alkanolamine (monoethanolamine etc.) solutions followed by regeneration of solvent by desorption. However, monoethanolamine (MEA), which is commonly used as the benchmark solvent, has a CO_2 loading ratio limited to a maximum of 0.5 mole CO_2/mole amine and the reversible reaction temperature range of 120–130 °C prompts high energy consumption during solvent regeneration. Because of the high energy requirements of this solvent system (especially the "reboiler duty"), there are intensified studies to design effective solvents to increase the CO_2 absorption capacity and reaction kinetics and also to reduce the latent heat requirement of aqueous systems.[3] The most important criteria for suitable solvents are low oxidative degradation rate, low volatility, low corrosiveness, and low energy consumption in the process. Carbon dioxide can also be removed from postcombustion flue gas by using other regenerable (switchable) solvents. For instance, carbon dioxide binding organic liquids (CO_2BOLs) are nonaqueous, chemically selective CO_2-separating solvents composed of an alcohol and a strong amidine or guanidine base. While a carbamate or bicarbonate ion is formed by the reaction of aqueous alkanolamine solutions with CO_2, an amidinium or guanidinium alkylcarbonate salts occur, depending on the base, when CO_2 is captured by CO_2BOLs and an ionic liquid is formed that causes a notable increase in polarity. As reported by Heldebrant et al., alkyl carbonate salts formed from CO_2BOLs do not form as many hydrogen bonds as carbamate and bicarbonate salts do.[4] This implies that the binding enthalpy of CO_2 decreases and the desorption process can be carried out at low temperatures.[5] This provides a less energy consuming process during the regeneration as in most of the cases CO_2 can be separated and switch the nonionic lean solvents by modest heating or simple inert gas bubbling. CO_2BOLs have tunable physicochemical properties and they remain liquid in the process and undergo dramatic changes in polarity with and without CO_2. The main advantages of CO_2BOLs are their high boiling points, low vapor pressures, good physical and chemical absorption capacities, lower heat capacities, and noncorrosive nature.[4]

In the last decade, there have been a number of theoretical studies performed at various levels of theory to investigate CO_2 absorption by different solvents.[6–10] Among those, Wang et al. suggested the single-step termolecular reaction mechanism for CO_2 capture by a mixture of DBU and propanol at the B3LYP/6-31G(d) level of theory with PCM approach to be the favorable one according to their kinetic parameter findings.[11]

As a continuation of our previous studies on similar systems, we experimentally and theoretically investigated the structural and energetic details of the single-step termolecular reaction mechanism for CO_2/DBN/1-propanol and CO_2/TBD/1-butanol systems and report our findings in the following sections.[12–15]

2. Results and discussion

2.1. Analysis

Previously, CO_2-amine reactions were unanimously considered to be direct carbamate formation followed by protonation of another amine. This led to a reaction rate expression that was first order both in CO_2 and in amine with a unity stoichiometric coefficient. However, this mechanism could not explain the fractional orders between 1 and 2 for certain amines. Therefore, mechanisms based on an unstable intermediate were introduced even though one of them involved two amines and one CO_2; that is a termolecular reaction normally considered unlikely. Surprisingly, a rare DFT study supported the termolecular reaction.[11,16,17] Since then, it has become usual to interpret the reaction of CO_2 with amines by both the zwitterion and the termolecular reaction mechanisms. The zwitterion mechanism was originally proposed by Caplow, and then reintroduced by Danckwerts.[18,19] This reaction mechanism, also known as a two-step mechanism, involves two sequential reactions. In the first step, CO_2 reacts with the amine and a zwitterion intermediate product is produced.

Then, in the second step, this zwitterion reacts further with a base (a water molecule, an additional amine, or any other basic species can also act as the base) and the base-catalyzed deprotonation of the zwitterion takes place to produce a carbamate ion and a protonated base.[3,20,21]

The termolecular reaction mechanism was first proposed by Crooks and Donnellan and later was modified significantly by da Silva and Svendsen.[6] Recently, Ozturk et al. reviewed the termolecular kinetic model for carbon dioxide binding organic liquids and described the mechanism in detail.[21,22] The termolecular reaction mechanism, which is easier to handle, assumes that an amine reacts simultaneously with both one molecule of carbon dioxide and one molecule of a base (B) in a single step to form a weakly bound intermediate product as illustrated in Figure 1. However, regardless of the mechanism, a carbamate and a protonated base are the generally accepted products of CO_2-amine reactions. It is also assumed that the reaction takes place via an intermediate as shown in Eq. (1).

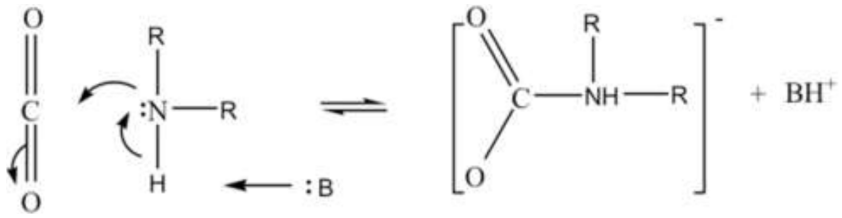

Figure 1. Schematic drawing of a termolecular reaction mechanism.[45]

$$CO_2 + RNH_2 \cdots B \rightleftarrows RNHCOO^- \cdots BH^+ \tag{1}$$

The modified termolecular reaction mechanism can be adapted to CO_2 BOL systems, containing amidine/guanidine base and a linear alcohol, as shown in Eqs. (2) and (3).

$$CO_2(g) + DBN_{(l)} + ROH_{(l)} \rightleftarrows [DBNH^+][ROCOO^-]_{(l)} \tag{2}$$

$$CO_2(g) + TBD_{(s)} + ROH_{(l)} \rightleftarrows [TBDH^+][ROCOO^-]_{(l)} \tag{3}$$

While a fraction of the resulting intermediate breaks up to form reactant molecules, a smaller fraction reacts further with a second molecule of organic base or alcohol to form ionic products (carbamate or bicarbonates). Under pseudo-first–order conditions, the observed forward reaction rate can be expressed as in Eq. (4):

$$r_{obs} = k_o[CO_2] \tag{4}$$

For a CO_2 BOL system, the observed reaction rate constant (k_o) for the mentioned mechanism can be expressed by Eqs. (5) and (6).

$$k_o = \{ k_{DBN}[DBN] + k_{ROH}[ROH] \} [DBN] \tag{5}$$

$$k_o = \{ k_{TBD}[TBD] + k_{ROH}[ROH] \} [TBD] \tag{6}$$

Since alcohol concentration is assumed to be in excess for the pseudo-first–order conditions, ROH can be considered constant and a new rate constant, k, can be defined by Eq. (7):

$$k = k_{ROH}[ROH] \tag{7}$$

$$k_o = \{ k_{DBN} [DBN] + k \} [DBN] \tag{8}$$

$$k_o = \{ k_{TBD} [TBD] + k \} [TBD] \tag{9}$$

As seen in Eqs. (8) and (9), the degree of the reaction can change between 1 and 2 depending on the rate of the reaction. If the alcohol is the dominant base, the system exhibits a first-order reaction and the above-mentioned equations reduce to Eqs. (10) and (11):

$$k_o = k [DBN] \tag{10}$$

$$k_o = k [TBD] \tag{11}$$

If amine (DBN, TBD in this study) is the dominant base, then the system exhibits second order with respect to amine and Eqs. (8) and (9) reduce to Eqs. (12) and (13):

$$k_o = k_{DBN} [DBN]^2 \tag{12}$$

$$k_o = k_{TBD} [TBD]^2 \tag{13}$$

In summary, the rate constants of CO_2 BOLs were obtained by using Eqs. (5)–(13).

2.2. Kinetic results

In this work, novel CO_2 BOLs composed of mixture of an organic base (as an amidine; DBN (1,5-Diazabicyclo[4.3.0] non-5-ene) and as a guanidine; TBD (1,5,7-Triazabicyclo[4.4.0]dec-5-ene) in 1-propanol and 1-butanol were developed. The reaction kinetics and activation energies of these switchable solvents were examined in order to evaluate the potential integration to industrial carbon dioxide capture applications. Intrinsic reaction rates were measured directly in the stopped flow equipment for a temperature range of 298–308 K. Organic base (amidine or guanidine) percentages in 1-propanol and 1-butanol medium varied from 2.5 wt% to 15.0 wt.%.

Table 1 shows the observed pseudo-first–order reaction rate constants for the CO_2/DBN/1-propanol system versus the weight-percent concentration of DBN at temperatures ranging from 288 K to 308 K. As expected, the observed reaction rate constants, in terms of k_o, increase as both the concentration of DBN and the temperature increase over 2.5–15.0 weight percentages and 288–308 K, respectively.

Table 1. Observed pseudo-first–order rate constants for the CO_2/DBN/1-propanol system at various temperatures.

k_o [s^{-1}]					
DBN [wt.%]	2.5	5	7.5	10	15
288 K	40.3	71.7	121.1	172.8	257.6
298 K	95.9	273.9	320.8	510.3	705.7
308 K	120.3	326.1	443.3	638.1	763.1

In order to determine the reaction order of the CO_2/DBN/1-propanol system, the natural logarithms of observed reaction rate constants versus DBN concentrations were plotted at various temperatures as shown in Figure 2. Empirical power law kinetics was fitted to the lines in Figure 2 by using the least square method. Their slopes correspond to the reaction orders of the CO_2/DBN/1-propanol system, which are determined

to be approximately 1.00 with regression values of R^2 = 0.97–0.99 for the 2.5–15.0 weight percentages at a temperature range of 288–308 K. The experimentally observed k_o values were correlated using a single-step termolecular mechanism to determine the forward reaction rate constant k [m^3 $kmol^{-1}$ s^{-1}]. The reaction rate constants vs. DBN concentrations were plotted according to Eq. (6) in a very satisfactory pseudo-first–order plot as seen in Figure 3. From the slopes of the fitted lines in Figure 3, the first-order forward reaction rate constants for CO_2/DBN/1-hexanol systems were determined to be 254.4 m^3 $kmol^{-1}$ s^{-1} at 288 K, 720.2 m^3 $kmol^{-1}$ s^{-1} at 298 K, and 843.3 m^3 $kmol^{-1}$ s^{-1} at 308 K.

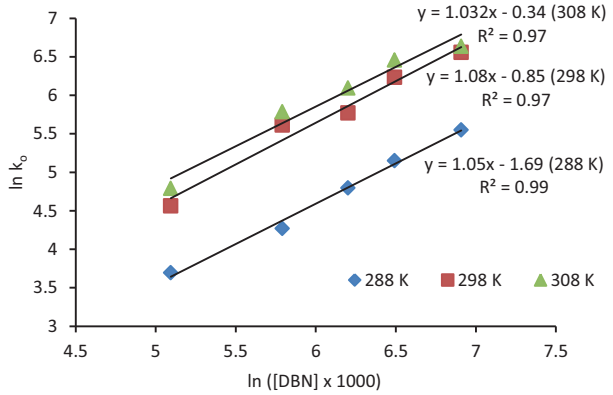

Figure 2. Determination of the apparent reaction order for the CO_2/DBN/1-propanol system at various temperatures.

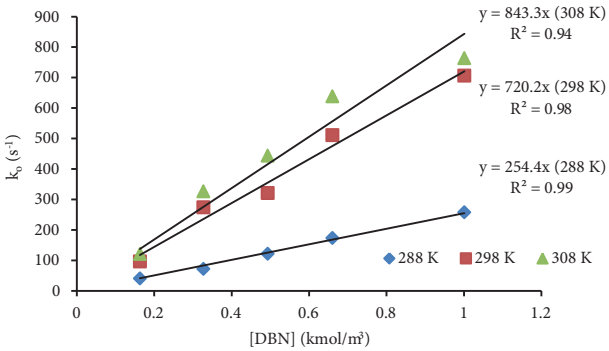

Figure 3. Pseudo-first–order rate constant as a function of DBN concentration at various temperatures.

In a similar fashion, the observed pseudo-first–order rate constants for the CO_2/TBD/1-butanol system versus the weight-percent concentration of TBD at 288, 298, and 308 K are summarized in Table 2.

Table 2. Summary of measured k_o values for the CO_2/TBD/1-butanol system at 288–308 K.

k_o [s^{-1}]				
TBD [wt.%]	2.5	5	7.5	10
288 K	211.1	399.1	711.1	781.5
298 K	380.1	925.7	1060.8	1735.1
308 K	621.2	1180.3	2149.5	2326.2

The reaction orders and the forward reaction rate constants k [m^3 $kmol^{-1}$ s^{-1}] of the CO_2/TBD/1-butanol system were calculated with the same procedure as mentioned above.

Table 3 shows a strong temperature dependency of the forward reaction rate constant.

Table 3. Summary of the reaction orders and the forward reaction rate constants of the CO_2/TBD/1-butanol system at 288–308 K.

TBD		
	k [m^3/kmol.s]	Reaction order
288 K	1402	0.98
298 K	2764.1	1.02
308 K	4190.3	0.99

2.3. Activation energies

Activation energies were obtained from Arrhenius plots according to Eq. (14):

$$k = A \exp\left(-\frac{E_a}{RT}\right), \tag{14}$$

where A is the Arrhenius constant (m^3/mol s) and E_a is the activation energy (kJ/mol).

Figure 4 shows the Arrhenius plot for the CO_2/DBN/1-propanol system at 2.5, 5.0, 7.5, 10.0, and 15 wt%, respectively. Using the slopes of fitted lines, activation energies for the CO_2/DBN/1-propanol system were calculated as 40.56 kJ/mol at 2.5 wt%, 56.31 kJ/mol at 5.0 wt%, 48.09 kJ/mol at 7.5 wt%, 48.51 kJ/mol at 10.0 wt%, and 40.41 kJ/mol at 10.5 wt%.

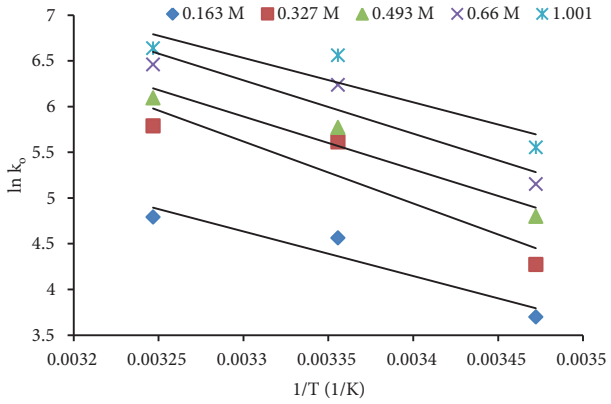

Figure 4. Arrhenius diagram for the CO_2/DBN/1-propanol system.

The same procedure was applied for the CO_2/TBD/1-butanol system. Activation energies for the CO_2/TBD/1-butanol system were calculated as 39.82 kJ/mol at 2.5 wt.%, 39.38 kJ/mol at 5.0 wt.%, 40.65 kJ/mol at 7.5 wt.%, and 40.41 kJ/mol at 10.0 wt.%.

Finally, the results obtained in this work were compared with published papers about other CO_2 BOLs at 298 K as shown in Table 4.

Table 4. Comparison of kinetic properties of various CO_2 BOLs.

Amines	DBN/1-propanol	TBD/1-butanol	DBN/1-hexanol[a]	TBD/1-hexanol[a]	BTMG/1-hexanol[a]	TMG/1-hexanol[b]	DBU/1-hexanol[c]
Reaction $order_{298K}$	1.08	1.02	1.09	0.63	0.83	0.98	1.21
k_{298} (m^3 $kmol^{-1}$ s^{-1})	720.2	2764.1	524.46	727.16	3122.2	64.10	627.0
Ea (kJ mol^{-1})	46.78	40.07	35.13	30.74	46.31	9.76	13.7

[a]:Yuksel Orhan et al. (2015), [b]: Ozturk et al. (2014), [c]: Ozturk et al. (2012).

However, the k_o values are generally low in comparison with those in MEA or PZ systems but they are comparable to those in aqueous DEA systems.[20,23–26] Nevertheless, the BTMG/1-hexanol system has the highest reaction rate, and is comparable with several commercial amine systems.

2.4. Computational results

According to the thermodynamic and kinetic analyses in a computational study on the DBU/1-hexanol/CO_2 system in the literature, the single-step termolecular reaction mechanism was the most feasible one.[11] Therefore,

we followed the same mechanism in the computational part of this study and investigated the interaction of the organic bases DBN and TBD with linear alcohols (1-propanol and 1-butanol, respectively) and CO_2 at different calculation levels of theory. Reactant, transition state, and product structures of the CO_2/DBN/1-propanol and CO_2/TBD/1-butanol systems obtained from the RB3LYP/6-311++G(d,p) level calculations with implicit inclusion of the solvent effects of 1-propanol and 1-butanol through the PCM are presented in Figure 5.

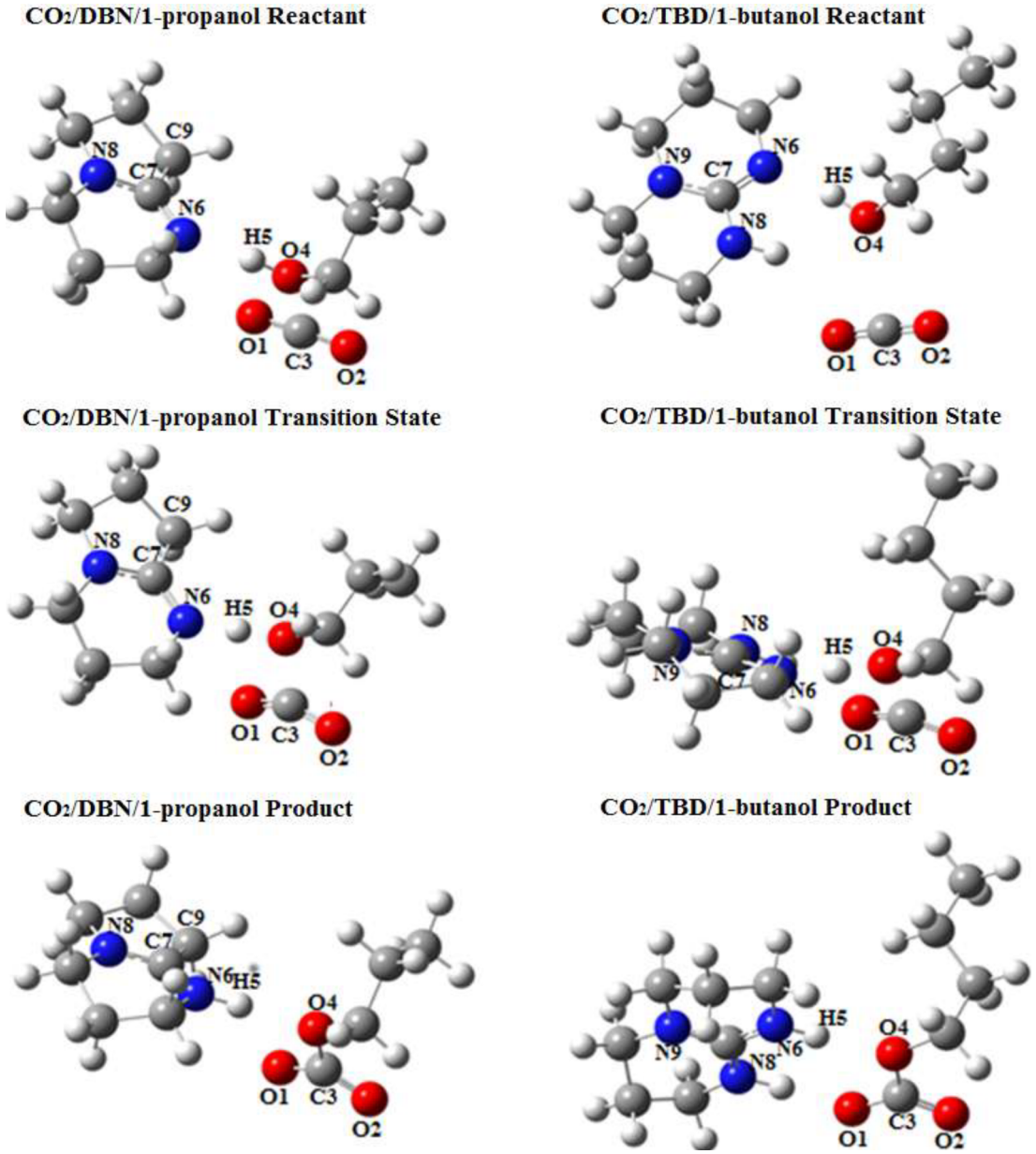

Figure 5. RB3LYP/6-311++G(d,p) calculated structures of reactants, transition states, and products for the CO_2/DBN/1-propanol and CO2/TBD/1-butanol systems with the PCM approach.

The geometrical parameters given in Table 5 are defined by using the atom labeling scheme presented on the transition structures of the CO_2/DBN/1-propanol and CO_2/TBD/1-butanol systems in Figure 5. It should be noted that the same labeling procedure is also used for reactant and product structures of these systems.

Table 5. Geometrical parameters (bond lengths in Å, bond angles in °) from RB3LYP/6-31G(d) and RB3LYP/6-311++G(d,p) with PCM calculations for CO_2/DBN/1-propanol and CO_2/TBD/1-butanol systems.

CO_2/DBN/1-propanol						
	Reactant		TS		Product	
Geometrical parameter	RB3LYP/ 6-31G(d)	RB3LYP/ 6-311++G(d,p)	RB3LYP/ 6-31G(d)	RB3LYP/ 6-311++G(d,p)	RB3LYP/ 6-31G(d)	RB3LYP/ 6-311++G(d,p)
H5–N6	1.785	1.793	1.352	1.323	1.035	1.030
H5–O4	0.998	0.994	1.142	1.167	1.765	1.801
C3–O4	2.660	2.767	1.847	1.881	1.459	1.439
C3–O2	1.169	1.161	1.198	1.189	1.239	1.239
C3–O1	1.169	1.161	1.199	1.189	1.245	1.243
O1–C3–O2	175.40	176.74	148.89	150.36	132.33	131.40
CO_2/TBD/1-butanol						
H5–N6	1.751	1.759	1.432	1.355	1.026	1.022
H5–O4	1.004	0.997	1.107	1.150	1.858	1.895
C3–O4	2.736	2.817	1.905	1.949	1.430	1.418
C3–O2	1.169	1.160	1.190	1.181	1.236	1.235
C3–O1	1.170	1.161	1.198	1.187	1.257	1.255
O1–C3–O2	176.60	177.21	151.50	153.27	130.31	129.90

The reactant structure of the CO_2/DBN/1-propanol system has an H5–O4 bond length of 0.994 Å at the RB3LYP/6-311++G(d,p) level of theory (and 0.998 Å at the RB3LYP/6-31G(d) level) where the CO_2/TBD/1-butanol system has 0.997 Å (and 1.004 Å at the RB3LYP/6-31G(d) level). The same geometrical parameter was calculated to be 1.167 Å (and 1.142 Å) and 1.150 Å (and 1.107 Å) for the transition state structure of the CO_2/DBN/1-propanol and CO_2/TBD/1-butanol systems, respectively, at the RB3LYP/6-311++G(d,p) level (and RB3LYP/6-31G(d) level). After the termolecular reaction took place, the distance between the H5 and O4 atoms was measured to be 1.801 Å (and 1.765 Å) for the CO_2/DBN/1-propanol and 1.895 Å (and 1.858 Å) for CO_2/TBD/1-butanol system. At the same time, the H5–N6 distance of 1.793 Å (1.785 Å) in the reactant decreases to 1.030 Å (1.035 Å) in the product structure of the CO_2/DBN/1-propanol system, and again this parameter decreases from 1.759 Å (1.751 Å) to 1.022 Å (1.026 Å) in the CO_2/TBD/1-butanol system. The O1–C3–O2 bond angle and C3–O4 distance for the CO_2/DBN/1-propanol reactant were calculated to be 176.74° (175.40°) and 2.767 Å (2.660 Å) and for its product calculated to be 131.40° (132.33°) and 1.439 Å (1.459 Å), respectively. The same decreasing trend in the O1–C3–O2 bond angle and C3–O4 distance from reactant to product was also obtained for the CO_2/TBD/1-butanol system. All these findings indicated that the H5–O4 bond was broken and new H5–N6 and C3–O4 bonds were formed during the termolecular reaction amongst amine, alcohol, and CO_2 molecules. The natural bond orbital analysis results, for reactant and product structures of both reaction systems given in Table 6, support the geometrical findings. Hydrogen transfer from alcohol to amine results in the diminishing of negative charges on N6 and N8 atoms and in the enhancement of the positive charge on the C7 atom from reactants to products for the CO_2/DBN/1-propanol and CO_2/TBD/1-butanol reaction systems at both levels of theory. In a similar way, the formation of new C3–O4 bonds between alcohol and CO_2 units causes the negative charges on O1 and O2 atoms to enhance significantly from reactant to product structure. For example, in the CO_2/DBN/1-propanol system, the negative charge on the O1 atom enhances from –0.518 e (–0.535 e) to –0.803 e (–0.793 e) at the RB3LYP/6-311++G(d,p) level (and at the RB3LYP/6-31G(d) level) of theory. The CO_2/TBD/1-butanol system also yields very similar results as given in Table 6. Enhancement of the negative charges on O1 and O2 atoms accompanied by lengthened C3–O1

and C3–O2 bond lengths, e.g., elongation from 1.161 Å to 1.243 Å for the C3–O1 bond and from 1.161 Å to 1.239 Å for the C3–O2 bond, was found for the CO_2/DBN/1-propanol system at the RB3LYP/6-311++G(d,p) level. On the other hand, the negative charge on the O4 atom was lessened for both reaction systems because of the weak interaction between O4 and H5 atoms in product structures. Our NBO analysis also revealed that in the product structure of the CO_2/DBN/1-propanol system partial charges for H bound DBN fragment and for newly bound CO_2/1-propanol fragment calculated to be 0.955e (0.929e) and –0.955 e (–0.929 e) at the RB3LYP/6-311++G(d,p) level (and at the RB3LYP/6-31G(d) level) of theory. For the CO_2/TBD/1-butanol system, we obtained 0.913 e (0.878 e) for H bound TBD fragment and –0.913e (–0.878e) for CO_2/1-butanol fragment. These findings indicate that the termolecular reaction mechanism yields zwitterionic products as defined by Eqs. (2) and (3) above.

Table 6. Partial charges (as e) of the atoms in the active field of the CO_2/DBN/1-propanol and CO_2/TBD/1-butanol systems obtained from NBO analysis at the RB3LYP/6-31G(d) and RB3LYP/6-311++G(d,p) levels with PCM (atom numbering scheme is given in Figure 6).

	CO_2/DBN/1-propanol				CO_2/TBD/1-butanol			
	Charge [RB3LYP/6-31G(d)]		Charge [RB3LYP/6-311++G(d,p)]		Charge [RB3LYP/6-31G(d)]		Charge [RB3LYP/6-311++G(d,p)]	
Atom	Reactant	Product	Reactant	Product	Reactant	Product	Reactant	Product
O1	–0.535	–0.793	–0.518	–0.803	–0.533	–0.797	–0.517	–0.819
O2	–0.532	–0.779	–0.517	–0.795	–0.528	–0.764	–0.514	–0.775
C3	1.051	1.008	1.030	0.992	1.051	1.021	1.027	1.006
O4	–0.827	–0.676	–0.833	–0.684	–0.838	–0.658	–0.840	–0.665
H5	0.503	0.476	0.499	0.463	0.505	0.461	0.498	0.446
N6	–0.627	–0.580	–0.650	–0.573	–0.675	–0.637	–0.689	–0.626
C7	0.480	0.554	0.496	0.571	0.644	0.693	0.659	0.707
N8	–0.463	–0.406	–0.497	–0.432	–0.675	–0.639	–0.657	–0.629
C9	–0.501	–0.508	–0.422	–0.428	–	–	–	–
N9	–	–	–	–	–0.494	–0.459	–0.527	–0.485

Activation energies of the CO_2/DBN/1-propanol and CO_2/TBD/1-butanol systems for the termolecular reaction mechanism were obtained from the single-point energy and frequency calculations on optimized reactant and product structures and additionally performing transition state and IRC calculations. Theoretical Gibbs free energy of activation values were obtained at 298 K initially with the RB3LYP/6-31G(d) and RB3LYP/6-311++G(d,p) level calculations with the PCM approach. Thereafter, activation energies were refined at the RMP2/6-31G(d)//RB3LYP/6-31G(d), RMP2/6-31G(d)//RB3LYP/6-311++G(d,p), RMP2/6-311++G(d,p)//RB3LYP/6-31G(d), and RMP2/6-311++G(d,p)//RB3LYP/6-311++G(d,p) levels with implicit inclusion of the solvent effects of 1-propanol and 1-butanol through the PCM approach again. Table 7 presents a comparison of theoretical and experimental Ea values, which are all obtained in this study. According to these energetic findings, it is clear that it is vital to refine the RB3LYP energies by using a higher level method, RMP2. Mean signed error (MSE) values indicate the underestimation tendency of all methods used in this study. This tendency is definitely less pronounced for RMP2/6-311++G(d,p)//RB3LYP/6-31G(d) with an MSE of –2.08 kJ mol^{-1}. On the other hand, RMP2/6-311++G(d,p)//RB3LYP/6-311++G(d,p) level was superior for Ea calculations with a mean unsigned error (MUE) of 3.28 kJ mol^{-1} and with a root-mean-square deviation (RMSD) of 4.27 kJ mol^{-1}. As we mentioned in our previous study, the coupled cluster method with single

and double excitations (CCSD) produces high errors for activation energies of similar termolecular systems.[15] Hence it was not taken into account during the Ea calculations in this study.

Table 7. Theoretical activation energies for the CO_2/DBN/1-propanol and CO_2/TBD/1-butanol systems obtained at various levels of theory and their deviations from the experiment (all in kJ mol^{-1}).

	CO_2/DBN/1-propanol		CO_2/TBD/1-butanol				
Calculation level	Ea	Error	Ea	Error	MSE	MUE	RMSD
RB3LYP/6-31G(d)	34.60	–12.18	25.66	–14.41	–13.3	13.3	13.34
RB3LYP/6-311++G(d,p)	40.57	–6.21	33.39	–6.68	–6.45	6.45	6.45
RMP2/6-31G(d)//RB3LYP/6-31G(d)	38.41	–8.37	41.29	1.22	–3.58	4.8	5.98
RMP2/6-31G(d)//RB3LYP/6-311++G(d,p)	36.42	–10.36	38.22	–1.85	–6.11	6.11	7.44
RMP2/6-311++G(d,p)//RB3LYP/6-31G(d)	40.63	–6.15	42.06	1.99	–2.08	4.07	4.57
RMP2/6-311++G(d,p)//RB3LYP/6-311++G(d,p)	40.77	–6.01	39.52	–0.55	–3.28	3.28	4.27
Experimental (see Table 4)	46.78		40.07				

3. Experimental

3.1. General

1,5-Diazabicyclo[4.3.0]non-5-ene with 98% purity (CAS no. 3001-72-7) and reagent grade 1,5,7-triazabicyclo[4.4.0]dec-5-ene with 99% purity (CAS no. 5807-14-7) were supplied by Sigma-Aldrich (St. Louis, MO, USA). 1-Butanol with $\geq$99.4% purity (CAS no. 71-36-3) and 1-propanol with $\geq$99.5% purity (CAS no. 71-23-8) were also obtained from Sigma-Aldrich. Carbon dioxide with a purity of 99.99% was obtained from Linde (Munich, Germany). Reagent grade chemicals were used without further purification.

3.2. Experimental method

In this work, the observed reaction rate constants of the homogeneous reaction between CO_2 and CO_2BOLs with temperatures ranging from 288 to 308 K were measured using a stopped-flow instrument (model SF-61SX2, manufactured by Hi-Tech Scientific, UK). This technique does not involve a gas absorption step and avoids the possible experimental errors caused by the depletion of the amine in the gas–liquid interface. Therefore, the mass resistance associated with the transfer of a gas component into the liquid phase does not take place.[27] This direct method of stopped flow equipment is not affected by the reversibility of the reaction or other influence parameters (e.g., CO_2 loading, viscosity, density, diffusivity). In addition, quick experiment run ($\sim$0.05 s), small amount of solvent consumption for each experimental run ($\sim$0.1 mL), and easy handling are other advantageous of this method.[28] The apparatus was made up of four main units: a sample handling unit, a conductivity detection cell, an A/D converter, and a microprocessor. A detailed description of the experimental arrangements of the stopped-flow equipment is given in the work by Alper.[29,30] During an experimental run, amine (DBN or TBD)/alcohol solution and freshly saturated carbon dioxide dissolved in alcohol were placed in sealed drive syringes in the sample unit. In each experimental run, a pneumatic air supply pushes two drive syringes into the conductivity detection cell. Equal volumes of solutions were mixed instantaneously in a cell for the reaction to occur and the flow was stopped. The ion formation initiates a voltage change, which is monitored as function of time continuously. The conductivity change as a function of time is measured by a circuit as described by Knipe et al., which gives an output voltage directly proportional to the solution conductivity.[31]

Then the equipment software Kinetic Studio calculates the observed pseudo-first–order reaction rate constant (k_o) of the rapid homogeneous reaction based on the exponential equation below:

$$Y = -A\exp(-k_o t) + Y_\infty, \tag{15}$$

where Y is the conductance (S), A is the amplitude of the signal (S), k_0 is the pseudo-first–order reaction rate constant (s^{-1}), t is the time (s), and Y_∞ is the conductance of the end of observed reaction (S).

A typical experimental output from the standard stopped flow system is shown in Figure 6, and a good agreement between the experimental data and the fitted function can be noted. To obtain consistent pseudo-first–order rate constants (k_o), experiments were repeated at least 10 times at each temperature for all concentrations. To satisfy the pseudo-first–order conditions, amine and alcohol concentrations were always much in excess of that of CO_2 (usually the molar ratio was at least 10:1).[27]

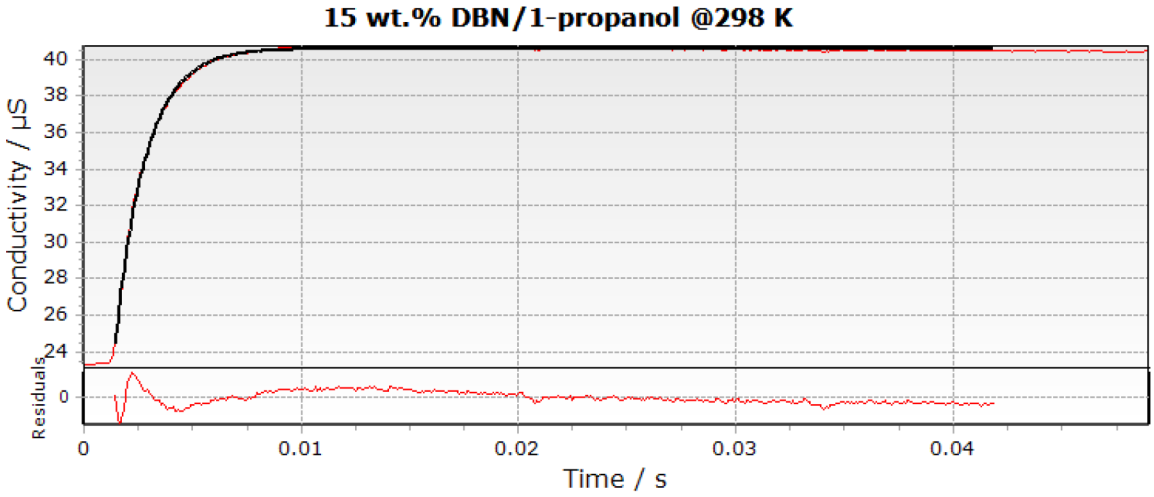

Figure 6. Combined average graphs of 15 wt.% DBN/1-propanol system at 298 K.

3.3. Computational method

In the second part of the study, we theoretically investigated the termolecular reaction mechanism for CO_2/DBN/1-propanol and CO_2/TBD/1-butanol systems with the help of quantum chemical calculations. Possible confirmations of all isolated amine and alcohol structures, which were later used to compose reactant and product structures, were prepared and optimized separately at the RB3LYP/6-31G(d) level of theory.[32–36] Appropriate energy minimum conformers were verified by vibrational frequency analyses and also zero point vibrational energies from these calculations were considered in the comparison of relative energies. In the next step, we prepared the reactant and product structures of the CO_2/DBN/1-propanol and CO_2/TBD/1-butanol termolecular reaction systems. All of these reactant and product structures were optimized at the RB3LYP/6-31G(d) and RB3LYP/6-311++G(d,p) levels of theory by including the solvent effect of 1-propanol and 1-butanol through the polarizable continuum model (PCM).[37–39] Following the geometry optimizations, vibrational frequency analyses were performed at the same levels on reactant and product structures to verify that all structures were proper minima on the potential energy surface with 3N-6 real vibrational frequencies, where N is the total number of atoms in the reaction system. To be able to find theoretical reaction barriers for each of the termolecular reaction systems, we performed transition state calculations and obtained Gibbs free energy of activation values

through the thermodynamic data produced. For both systems, intrinsic reaction coordinate (IRC) calculations were also performed to verify that the TS structures obtained for each of the reaction systems are connected to two specific minima on the reaction coordinate. Next, charge distributions on reactants and products were obtained for each reaction system by performing natural bond orbital (NBO) analysis. In addition to energetic findings, geometrical parameters for all reactant, transition state, and product structures were also found by using RB3LYP/6-31G(d) and RB3LYP/6-311++G(d,p) calculations with the PCM. Finally, single point energy calculations on optimized reactant, transition state, and product structures were performed at the higher levels of theory, RMP2/6-31G(d)//RB3LYP/6-31G(d), RMP2/6-31G(d)//RB3LYP/6-311++G(d,p), RMP2/6-311++G(d,p)//RB3LYP/6-31G(d), and RMP2/6-311++G(d,p)//RB3LYP/6-311++G(d,p) with the inclusion of PCM, to refine the computed activation energy values. The Gaussian 09 quantum chemistry software package was used to perform DFT and RMP2 calculations, and GaussView 5.0.9 was utilized for 3D molecular visualizations.[40−44]

In conclusion, we investigated the potential use of two new carbon dioxide binding organic liquids in CO_2 capture through experimental reaction kinetic studies and quantum chemical calculations. A termolecular reaction mechanism was used to obtain reaction rate constants and reaction barriers for the CO_2/DBN/1-propanol and CO_2/TBD/1-butanol reactions. Our findings indicated that the TBD/1-butanol system has a lower reaction barrier and faster reaction kinetics than the DBN/1-propanol system. Structural details of the single-step termolecular reaction mechanism were clarified by the quantum chemical studies, and good agreement between RMP2/6-311++G(d,p)//RB3LYP/6-311++G(d,p) level calculations and experiments was found for the activation energies of both systems investigated.

Acknowledgments

This work was supported by the Scientific and Technological Research Council of Turkey (TÜBİTAK) through a research project (Project No.: 213M390). The authors gratefully acknowledge this financial support.

Nomenclature

CO_2BOLs	Carbon dioxide binding organic liquids
CCS	Carbon capture and storage
B	Base (i.e. amine, water, or hydroxyl ion)
CO_2	Carbon dioxide
DBN	1,5-Diazabicyclo[4.3.0]non-5-ene
DBU	1,8-Diazabicyclo [5.4.0] undec-7-ene
DEA	Diethanolamine
GHG	Greenhouse gas
Ea	Activation energy
IRC	Intrinsic reaction coordinate
k_{OH}	Rate constant for alcohol, m^3/kmol·s
k_B	Rate constant for base according to Eq. (7), m^3/kmol·s
k_o	Observed pseudo-first–order rate constant, s^{-1}
MDEA	Methyldiethanolamine
MEA	Monoethanolamine
NBO	Natural bond orbital
SCC	Stress corrosion cracking
TBD	1,5,7-Triazabicyclo[4.4.0]dec-5-ene
TMG	1,1,3,3-Tetramethylguanidine

References

1. Thiruvenkatachari, R.; Su, S.; An, H.; Yu, X. X. *Prog. Energ. Combust.* **2009**, *35*, 438-455.
2. Liu, H.; Sema, T.; Liang, Z.; Fu, K.; Idem, R.; Na, Y.; Tontiwachwuthikul, P. *Sep. Purif. Technol.* **2014**, *136*, 81-87.
3. Yüksel Orhan, Ö.; Öztürk, M. Ç.; Şeker, A.; Alper, E. *Turk. J. Chem.* **2015**, *39*, 13-24.
4. Heldebrant, D. J.; Yonker, C. R.; Jessop, P. G.; Phan, L. *Energy Procedia* **2009**, *1*, 1187-1195.
5. Jessop, P. G.; Mercer, S. M.; Heldebrant, D. J. *Energy Environ. Sci.* **2012**, *5*, 7240-7253.
6. da Silva, E. F.; Svendsen, H. F. *Ind. Eng. Chem. Res.* **2004**, *43*, 3413-3418.
7. Pérez, E. R.; Santos, R. H. A.; Gambardella, M. T. P.; de Macedo, L. G. M.; Rodrigunes-Filho, U. P.; Launay, J. C.; Franco, F. D. *J. Org. Chem.* **2004**, *69*, 8005-8011.
8. Ochiai, B.; Yokota, K.; Fujii, A.; Nagai, D.; Endo, T. *Macromolecules* **2008**, *41*, 1229-1236.
9. Pereira, F. S.; de Azevedo, E. R.; da Silva, E. F.; Bonagamba, T. J.; da Silva Agostini, D. L.; Magalhanes, A.; Job, A. E.; Pérez Gonzalez, E. R. *Tetrahedron* **2008**, *64*, 10097-10106.
10. Yamada, H.; Matsuzaki, Y.; Higashii, T.; Kazama, S. *J. Phys. Chem. A* **2011**, *115*, 3079-3086.
11. Wang, Y.; Han, Q.; Wen, H. *Mol. Simulat.* **2013**, *10*, 822-827.
12. Kayi, H.; Kaiser, R. I.; Head, J. D. *Phys. Chem. Chem. Phys.* **2011**, *13*, 11083-11098.
13. Kayi, H.; Kaiser, R. I.; Head, J. D. *Phys. Chem. Chem. Phys.* **2011**, *13*, 15774-15784.
14. Kayi, H.; Kaiser, R. I.; Head, J. D. *Phys. Chem. Chem. Phys.***2012**, *14*, 4942-4958.
15. Yuksel Orhan, O.; Tankal, H.; Kayi, H.; Alper, E. *Int. J. Greenh. Gas Cont.* **2016**, *49*, 379-386.
16. Couchaux, G.; Barth, D.; Jacquin, M.; Faraj, A.; Grandjean, J. *Oil Gas Sci. Technol. - Rev. IFP* **2014**, *69*, 865-884.
17. Vaidya, P. D.; Kenig, E. Y. *Chem. Eng. Technol.* **2010**, *33*, 1577-1581.
18. Caplow, M. *J. Am. Chem. Soc.* **1968**, *90*, 6795-6803.
19. Danckwerts, P. V. *Chem. Eng. Sci.* **1979**, *34*, 443-446.
20. Cullinane, J. T.; Rochelle, G. T. *Fluid Phase Equilibria* **2005**, *227*, 197-213.
21. Ozturk, M. C.; Yuksel Orhan, O.; Alper, E. *Int. J. Greenh. Gas Cont.* **2014**, *26*, 76-82.
22. Ozturk, M. C.; Ume, C. S.; Alper, E. *Chem. Eng. Technol.* **2012**, *35*, 2093-2098.
23. Gordesli, F. P.; Ume, C. S.; Alper, E. *Inter. J. Chem. Kinet.* **2013**, *45*, 566-573.
24. Ume, C. S.; Ozturk, M. C.; Alper, E. *Chem. Eng. Technol.* **2012**, *35*, 464-468.
25. Orhan, O. Y.; Alper, E. *Chem. Eng. Technol.* **2015**, *38*, 1485-1489.
26. Siemieniec, M.; Kierzkowska-Pawlak, H.; Chacuk, A. *Ecol. Chem. Eng. S* **2012**, *19*, 55-66.
27. Kierzkowska-Pawlak, H.; Siemieniec, M.; Chacuk, A. *Chem. Pap.* **2013**, *67*, 1123-1129.
28. Rayer, A. V.; Henni, A.; Li, J. L. *Can. J. Chem. Eng.* **2013**, *91*, 490-498.
29. Alper, E. *Chem. Eng. J. Bioch. Eng.* **1990**, *44*, 107-111.
30. Alper, E. *Ind. Eng. Chem. Res.* **1990**, *29*, 1725-1728.
31. Knipe, A. C.; Mclean, D.; Tranter, R. L. *J. Phys. E Sci. Instrum.* **1974**, *7*, 586-590.
32. Harihara, P. C.; Pople, J. A. *Theor. Chim. Acta* **1973**, *28*, 213-222.
33. Becke, A. D., *Phys. Rev. A* **1988**, *38*, 3098-3100.
34. Lee, C. T.; Yang, W. T.; Parr, R. G., *Phys. Rev. B* **1988**, *37*, 785-789.
35. Becke, A. D. *J. Chem. Phys.* **1993**, *98*, 5648-5652.

36. Becke, A. D. *J. Chem. Phys.* **1993**, *98*, 1372-1377.

37. Krishnan, R.; Binkley, J. S.; Seeger, R.; Pople, J. A. *J. Chem. Phys.* **1980**, *72*, 650-654.

38. Frisch, M. J.; Pople, J. A.; Binkley, J. S. *J. Chem. Phys.* **1984**, *80*, 3265-3269.

39. Miertuš, S.; Scrocco, E.; Tomasi, J. *Chem. Phys.* **1981**, *55*, 117-129.

40. Møller, C.; Plesset, M. S. *Phys. Rev.* **1934**, *46*, 0618-0622.

41. Headgordon, M.; Pople, J. A.; Frisch, M. J. *Chem. Phys. Lett.* **1988**, *153*, 503-506.

42. Frisch, M. J.; Headgordon, M.; Pople, J. A. *Chem. Phys. Lett.* **1990**, *166*, 275-280.

43. Frisch, M. J.; Trucks, G. W.; Schlegel, H. B.; Scuseria, G. E.; Robb, M. A.; Cheeseman, J. R.; Scalmani, G.; Barone, V.; Mennucci, B.; Petersson, G. A.; Nakatsuji, H.; et al. *Gaussian 09*, *Revision A.1;* Gaussian: Wallingford, CT, USA, 2009.

44. Dennington, R., Keith T., Milliam J. *GaussView, Ver. 5.0.9*, Semichem Inc., Shawnee Mission, KS, USA, 2009.